frontiers | Frontiers in Earth Science

ORIGINAL RESEARCH
published: 04 July 2022
doi: 10.3389/feart.2022.927550

Electrical Conductivity of Eclogitic Omphacite and Garnet at Water-Rich Conditions

Hanyong Liu[1,2] *and Xiaozhi Yang*[1,2]*

[1]State Key Laboratory for Mineral Deposits Research, School of Earth Sciences and Engineering, Nanjing University, Nanjing, China, [2]Frontiers Science Center for Critical Earth Material Cycling, Nanjing University, Nanjing, China

Electrical conductivity of water-rich omphacite and garnet in eclogite was measured at 1 GPa and 200–800°C in a piston cylinder press and by a Solartron-1260 impedance/gain-phase analyzer at 10^6-1 Hz frequency. The water content of pre-annealed omphacite and garnet was 775–2,000 and 705–1,460 ppm H_2O, respectively. Sample chemistry and water contents remained unchanged during conductivity runs. At otherwise identical conditions, the conductivity of both minerals increases with both temperature and water content, and the water content exponent is ~1.45 and 1.12 for omphacite and garnet, respectively. The activation enthalpy is ~70 kJ/mol for omphacite and 84 kJ/mol for garnet and is broadly independent of sample water content. Combining with previous work, the conductivity dependence of omphacite on water content differs between water-rich and water-poor conditions, due to different types and mobility of water in samples that are closely related to its incorporation mechanism; in contrast, the conductivity dependence of garnet with a similar type of water is comparable over a wide range of water contents. The estimated bulk conductivity of eclogite at water-rich conditions is very high, up to ~0.01–0.1 S/m at 600–900°C. Geophysically resolved high resistivity of subducting crusts at 70–120 km depth suggests extremely low water contents of omphacite and garnet in the eclogitized slab. The data provide support to the model based on omphacite and garnet conductivity at water-poor conditions that the amount of water recycled by crust subduction to the deep mantle is probably limited.

Keywords: water, electrical conductivity, omphacite, garnet, eclogite, crust subduction

OPEN ACCESS

Edited by:
Baohua Zhang,
Zhejiang University, China

Reviewed by:
Haihao Guo,
UMR7327 Institut des sciences de la Terre d'Orléans (ISTO), France
Ye Peng,
Florida State University, United States
Yongsheng Huang,
Guangzhou Institute of Geochemistry (CAS), China

***Correspondence:**
Xiaozhi Yang
xzyang@nju.edu.cn

Specialty section:
This article was submitted to Earth and Planetary Materials, a section of the journal Frontiers in Earth Science

Received: *24 April 2022*
Accepted: *23 May 2022*
Published: *04 July 2022*

Citation:
Liu H and Yang X (2022) Electrical Conductivity of Eclogitic Omphacite and Garnet at Water-Rich Conditions. Front. Earth Sci. 10:927550. doi: 10.3389/feart.2022.927550

INTRODUCTION

Electrical conductivity of a rock matrix is sensitive to the presence and character of water in the system. By combining laboratory conductivity measurements of Earth materials with geophysically resolved electrical structure of Earth's interior, the water content in the crust and mantle may be inferred (Karato, 2006). Eclogite, consisting mainly of omphacite and garnet, is the dominant constituent of subducting crusts exceeding about 30 km in depth where the eclogite–facies metamorphism occurs. In recent studies, it has been established that the conductivity of eclogitic omphacite and garnet is determined by Fe and water (structurally bound hydroxyl) in them (Liu et al., 2019; Zhang et al., 2019; Liu et al., 2021a). By considering the mineral chemistry of subducting crusts and the resolved electrical structure, Liu et al. (2021a) inferred that the water content of omphacite and garnet in the downgoing crust at 70–120 km depth is globally low, <400 and <80 ppm H_2O, respectively. This means extremely low water activity during the eclogite–facies

metamorphism and in the subducting crust and the absence of appreciated amounts of hydrous minerals in the system, indicating the limited role of crust subduction in transferring water to depths beyond ~70 km (Liu et al., 2021a).

The discovery of Liu et al. (2021a) relies on conductivity studies of samples with low water contents, ≤300 ppm H_2O in omphacite and ≤150 ppm H_2O in garnet. The water content of omphacite and garnet in subduction-related massif eclogites, that were once subducted to > 90 km depth and then exhumed to the surface by tectonic movements, is greater than 1,500 ppm H_2O (Langer et al., 1993; Katayama and Nakashima, 2003; Xia et al., 2005; Sheng et al., 2007). Under water-rich conditions, if the activation enthalpy of omphacite and garnet conductivity decreases strongly as reported for other minerals, such as olivine, wadsleyite, and ringwoodite (Yoshino et al., 2008; Poe et al., 2010), the conductivity at high temperature could be reduced to a level similar to that at water-poor conditions, and the conclusion of Liu et al. (2021a) may then not hold. Hence, a careful evaluation of omphacite and garnet conductivity under water-rich conditions is critical for assessing the deep recycling of water by crust subduction. In this study, we have experimentally measured the conductivity of omphacite and garnet in eclogite with up to ~2,000 ppm H_2O. The data demonstrate that the activation enthalpy of water-rich omphacite and garnet is not significantly reduced, relative to water-poor conditions, and the conductivity generally increases with increasing water content over a large variation. The results confirm the model given by Liu et al. (2021a) that oceanic crust subduction probably recycles a very limited amount of water into deep Earth.

EXPERIMENTS AND METHODS

Sample Characterizations

Starting omphacite and garnet were the same as those in the study by Liu et al. (2019) for conductivity runs at water-poor conditions and were separated by handpicking under a binocular microscope from a fresh eclogite sample from Weissenstein, Münchberger Gneiss Massif (Germany), a famous region related to slab subduction and exhumation (Franz et al., 1986). Compositions of the omphacite and garnet, especially Fe content, are moderate of those in global massif eclogites and are thus representative (Liu et al., 2019). Optically clear omphacite and garnet grains were annealed with minor distilled water in Ni capsules in a piston-cylinder press at 1–2 GPa and 750–900°C (80–120 h) to homogenize the water distribution. Annealed samples were ground to 30–80 μm in size and cold-pressed into 3 mm diameter and 1.6–1.8 mm length cylinders for subsequent conductivity experiments.

Sample chemistry was measured by a JXA-iSP100 Electron Microprobe, at 15 kV accelerating voltage, 20 nA beam current, and 5 μm beam diameter. The water content of omphacite and garnet was determined with a Bruker Vertex 70 V Fourier-transform infrared (FT-IR) spectrometer coupled to a Hyperion 2000 microscope. For anisotropic omphacite, pre-annealed relatively large grains were analyzed by a polarized beam along with three orthogonal directions of each grain (Shuai and Yang, 2017), and fine-grained samples after conductivity runs were measured by an unpolarized beam on ~15 randomly oriented crystals in each sample (Qiu et al., 2018). For cubic garnet, the samples were analyzed by an unpolarized beam and averaged over > five grains. A wire-grid ZeSe polarizer was used to generate the polarized beam. The Beer–Lambert law was used to calculate water content, and the mineral-specific integral molar absorption coefficients of Katayama et al. (2006) for eclogitic omphacite and garnet were applied. The uncertainty of water content arising from spectral baseline corrections is usually < 10%. The general results of this study are not affected by the choice of these calibration coefficients, as documented by Liu et al. (2019) and Liu et al. (2021a).

Impedance Measurements

Conductivity runs were conducted at 1 GPa in a piston-cylinder press. Impedance was measured with a Solartron 1260 Impedance/Gain-Phase Analyzer, with frequency sweeping at $10^6$1 Hz and 0.5 V applied voltage. The assembly design follows that in our previous studies (Yang et al., 2011, Yang et al., 2012; Yang, 2012; Yang and McCammon, 2012; Li et al., 2016; Li et al., 2017; Liu et al., 2019; Liu et al., 2021a; Liu et al., 2021b). In brief, BN-Ni double capsules were used, in which the sample, two Pt electrodes, Ni-NiO buffer pairs, and a type-S thermocouple were located. The assembly yields a relatively sealed chamber, which helps maintain sample geometry and buffer redox state, and sample Fe loss to Pt electrodes is negligible, as documented previously (Yang et al., 2011, Yang et al., 2012; Yang and McCammon, 2012; Liu et al., 2021b).

Before assembly, the Al_2O_3 parts were pre-heated at 1,000°C for ~4 h to remove absorbed water, and during assembly, no glue/cement was used to immobilize the various parts to avoid volatile release at a high temperature that influences impedance analyses. Upon finishing the assembly, it was heated at 136°C in an oven overnight. After loading the assembly into the press and reaching the target pressure, the sample was heated again at 200°C. To avoid water loss by diffusion, impedance spectra were recorded in different heating–cooling cycles at 200–800°C.

After each run, the recovered sample was polished for optical examination and FT-IR and microprobe analyses. In general, no other phases were observed, Ni–NiO pairs were present, and sample distortions were negligible. Conductivity (σ) was calculated by $\sigma = L/(A \cdot R)$, where L and A are the length and cross-section area of recovered samples (by considering the effective contact between sample and electrodes), respectively, and R is the resistance by fitting the high-frequency arc in the impedance spectra (as discussed below). Uncertainty is < 20°C for temperature, for example, the thermal gradient along the capsule length and is usually < 10% for conductivity (Yang et al., 2011; Yang et al., 2012; Yang and McCammon, 2012).

RESULTS

Sample chemistry demonstrates nearly no change during the conductivity runs (**Table 1**). FT-IR spectra of typical pre-

TABLE 1 | Composition of omphacite and garnet in eclogite (wt%).

Samples	Run no.	SiO_2	TiO_2	Al_2O_3	FeO	MnO	MgO	CaO	Na_2O	K_2O	Total
Starting material											
Omp[a]		55.64	0.07	11.38	4.27	0.02	8.44	12.98	7.31	<0.01	100.11
		0.16	*0.03*	*0.35*	*0.28*	*0.02*	*0.17*	*0.40*	*0.24*	*<0.01*	
Grt[a]		37.64	0.03	22.73	26.55	0.74	6.81	5.63	0.03	<0.01	100.16
		0.20	*0.02*	*0.12*	*0.36*	*0.08*	*0.17*	*0.32*	*0.02*	*<0.01*	
Recovered samples											
Omp	A241	55.43	0.08	11.17	4.37	0.01	8.51	12.59	7.23	0.01	99.39
		0.08	*0.03*	*0.06*	*0.15*	*0.01*	*0.31*	*0.33*	*0.07*	*0.01*	
	B335	55.43	0.08	11.47	4.12	0.01	8.86	12.79	7.13	0.01	99.89
		0.08	*0.03*	*0.36*	*0.10*	*0.01*	*0.04*	*0.53*	*0.03*	*0.01*	
	A257	55.35	0.03	11.79	4.49	0.02	8.28	12.78	7.01	0.01	99.77
		0.14	*0.01*	*0.20*	*0.16*	*0.01*	*0.06*	*0.11*	*0.05*	*<0.01*	
Grt	A261	37.78	0.02	22.59	26.58	0.67	6.70	5.54	0.02	<0.01	99.92
		0.13	*0.00*	*0.14*	*0.03*	*0.06*	*0.11*	*0.09*	*0.00*	*<0.01*	
	A275	37.68	0.08	22.67	26.60	0.37	6.52	5.46	0.01	<0.01	99.39
		0.12	*0.01*	*0.10*	*0.19*	*0.02*	*0.44*	*0.38*	*0.00*	*<0.01*	

[a]: *reproduced from Liu et al. (2019).*

Assuming all Fe as FeO. Data are expressed as the average and standard deviation (italic) by electron microprobe analyses. Omp, *omphacite;* Grt, *garnet.*

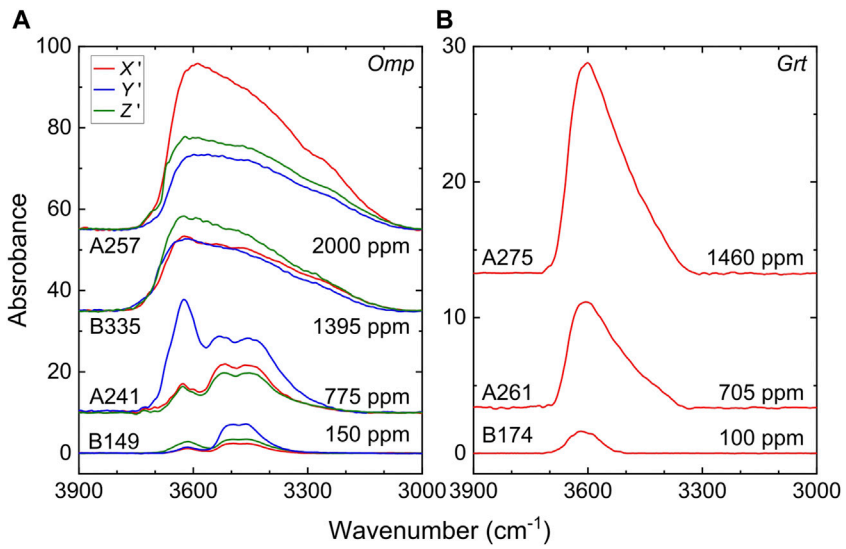

FIGURE 1 | Representative FT-IR spectra of pre-annealed omphacite and garnet. **(A)** Polarized spectra of omphacite along with three orthogonal directions (*X′*, *Y′*, and *Z′*) and **(B)** unpolarized spectra of garnet (see text). Spectra of 150 ppm H_2O omphacite and 100 ppm H_2O garnet (bottom in each panel) are from Liu et al. (2019). Spectra were normalized to 1 cm thickness and vertically offset. *Omp*, omphacite; *Grt*, garnet.

annealed samples are presented in **Figure 1**, along with the spectra of low water content samples from the study by Liu et al. (2019) for comparison. All spectra show OH bands at 3,700–3,100 cm^{-1}, with peaks located at ~3,620, 3,520, and 3,450 cm^{-1} in omphacite and ~3,605 cm^{-1} (asymmetric) in garnet, and shapes and frequency positions of the bands agree with those in previous reports for the corresponding natural and H-annealed minerals (Langer et al., 1993; Katayama and Nakashima, 2003; Xia et al., 2005; Katayama et al., 2006; Sheng et al., 2007; Schmädicke and Gose, 2017; Jiang et al., 2022). H_2O content is ~775, 1,395, and 2,000 ppm in omphacite and 705 and 1,460 ppm in garnet (**Table 2**). For omphacite, the spectral shapes differ between water-rich (775–2000 ppm H_2O, H-annealings at 750–900°C, this study) and water-poor (85–290 ppm H_2O, H-annealings at 650–700°C, Liu et al., 2019) conditions, with enhanced bands at ~3,620 cm^{-1} and broadened bands at 3,700–3,100 cm^{-1} in the former case; for garnet, spectral shapes are similar over a large variation in water content, except for broad bands at water-rich (705–1,460 ppm H_2O, H-annealings at 800–900°C) conditions.

Representative impedance spectra of the samples are shown in **Figure 2**. Usually, spectra show a high-frequency

TABLE 2 | Summary of samples and fitting parameters in conductivity runs.

Run No.	T (°C)	ppm H_2O		L/A (m^{-1})	$\log_{10}$ (σ_0 (S/m))	$\log_{10}$ (σ' 0 (S/m))	r	ΔH (kJ/mol)	ΔH_H (kJ/mol)
		initial	final						
Omphacite									
B185[a]	350–700	85	80	290	1.38 ± 0.24	—	—	84 ± 4	—
B149[a]	350–700	150	160	216	1.52 ± 0.14	—	—	82 ± 2	—
B145[a]	350–700	290	300	269	1.75 ± 0.12	—	—	81 ± 2	—
—	—	—	—	—	—	3.51 ± 0.11	1.10 ± 0.04	—	82 ± 1[b]
A241	200–800	775	795	274	1.89 ± 0.07	—	—	72 ± 1	—
B335	200–700	1395	1410	270	2.04 ± 0.05	—	—	70 ± 1	—
A257	200–600	2000	1985	296	2.37 ± 0.07	—	—	70 ± 2	—
—	—	—	—	—	—	3.36 ± 0.05	1.45 ± 0.04		71 ± 1[c]
Garnet									
B167[a]	350–800	40	45	226	1.80 ± 0.17	—	—	90 ± 3	—
B174[a]	350–800	100	95	245	2.26 ± 0.12	—	—	91 ± 2	—
—	—	—	—	—	—	4.37 ± 0.24	1.07 ± 0.09	—	90 ± 2[b]
A261	250–700	705	690	254	2.76 ± 0.11	—	—	84 ± 2	—
A275	250–700	1460	1465	290	3.08 ± 0.11	—	—	84 ± 1	—
—	—	—	—	—	—	4.02 ± 0.11	1.12 ± 0.08	—	84 ± 1[c]
—	—	—	—	—	—	4.25 ± 0.10	1.11 ± 0.05	—	87 ± 1[d]

Sample H_2O content is rounded to the nearest ~5 ppm. L/A is the sample dimension factor, and parameters are obtained by applying ***Eqs 1***, ***2*** *to measured data (see text).*
[a]*: samples reported by Liu et al. (2019).*
[b]*: by multilinear regression of water-poor samples as reported by Liu et al. (2019).*
[c]*: by multilinear regression of water-rich samples in this study.*
[d]*: by applying a global multilinear regression to both water-poor (Liu et al., 2019) and water-rich (this study) garnets (see text).*

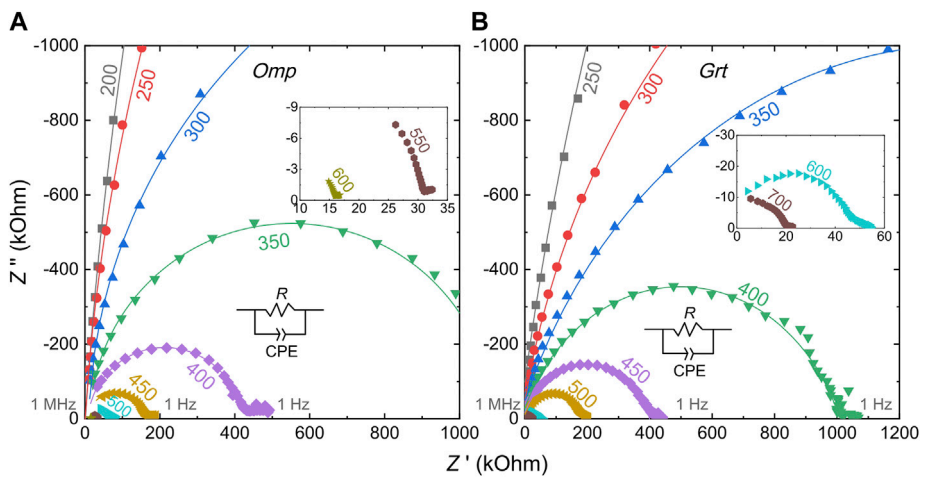

FIGURE 2 | Representative impedance spectra of **(A)** omphacite (A257) and **(B)** garnet (A275). Z′ and Z″ are the real and imaginary parts, respectively. An equivalent circuit of a single *R*-CPE circuit element, a resistor *R*, and a constant phase element (CPE) in parallel was used to fit the high-frequency arc in each spectrum. The number close to each spectrum is the temperature (°C), and insets show spectra at high temperatures. *Omp*, omphacite; *Grt*, garnet.

arc and a low-frequency short tail in each spectrum, resembling those reported for silicate minerals (Huebner and Dillenburg, 1995; Dai and Karato, 2009; Yoshino et al., 2009; Poe et al., 2010; Yang et al., 2011; Yang et al., 2012; Zhao and Yoshino, 2016; Li et al., 2017; Zhang et al., 2019; Liu et al., 2021b). The arc is commonly attributed to grain interior conduction and tail to sample-electrode reactions (or electrode effects). Conductivity (σ) of silicate minerals as a function of temperature is described by the Arrhenius relation:

$$\sigma = \sigma_0 \cdot \exp\left(-\frac{\Delta H}{RT}\right) \quad (1)$$

where σ_0 is the pre-exponential factor, ΔH is the activation enthalpy, R is the ideal gas constant, and T is the absolute temperature. Conductivity in the first heating cycle was

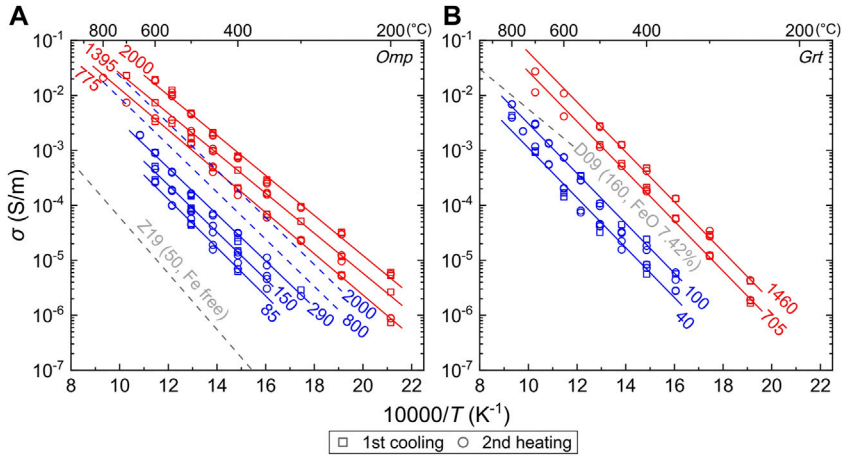

FIGURE 3 | Conductivity of **(A)** omphacite and **(B)** garnet. Red and blue denote water-poor and water-rich conditions, respectively, with water content shown (ppm H_2O) for each sample. **(A)** Red and blue solid lines are multilinear fittings by **Eq. 2** to the data of water-poor and water-rich samples, respectively, and dashed blue lines by applying the parameters of water-poor omphacite to water-rich conditions (see text). **(B)** Solid lines are multilinear fittings to the data of all samples, marked as red and blue for water-poor and water-rich samples, respectively. Uncertainty is usually smaller than symbol sizes. Compiled data: Z19, Zhang et al. (2019) at 3 GPa for a synthetic Fe-free omphacite (50 ppm H_2O); D09, Dai and Karato (2009) at 8 GPa for a pyrope (~7.42% FeO and 160 ppm H_2O). *Omp*, omphacite; *Grt*, garnet.

usually subjected to residual moistures in the system, yielding data not following **Eq. 1** as documented in similar work (Yoshino et al., 2009; Yang et al., 2012; Li et al., 2016; Li et al., 2017; Liu et al., 2019; Liu et al., 2021a; Liu et al., 2021b), and relevant data were excluded. The conductivity of samples and their fittings are plotted in **Figure 3**, and parameters by fitting the data to **Eq. 1** are summarized in **Table 2**. Data in each run are reproducible between different heating–cooling cycles. The obtained activation enthalpy is ~70 and 84 kJ/mol for omphacite and garnet, respectively (**Table 2**). The conductivity of both minerals increases with temperature and water content at otherwise identical conditions, which is in line with previous work on nominally anhydrous minerals (NAMs) (Dai and Karato, 2009; Yoshino et al., 2009; Poe et al., 2010; Yang et al., 2011; Yang et al., 2012; Yang and McCammon, 2012; Zhao and Yoshino, 2016; Liu et al., 2019; Liu et al., 2021a; Liu et al., 2021b; Zhang et al., 2019).

To quantify the effect of water content on sample conductivity, the data are further modeled by

$$\sigma = \sigma_0^{'} \cdot C_{\mathrm{H}}^{r} \cdot \exp\left(-\frac{\Delta H_{\mathrm{H}}}{RT}\right) \quad (2)$$

where σ' 0 is a constant, C_{H} is the water content, r is a factor linked to the nature of charged H species, and ΔH_{H} is the activation enthalpy. This assumes that conduction in the hydrous omphacite and garnet is dominated by protons (H) over the studied temperature range (see also discussion below). The parameters by applying **Eq. 2** to the samples, using a multilinear fitting to the data of each mineral, are given in **Table 2**. The yielded activation enthalpy (ΔH_{H}) and exponent (r) are ~71 kJ/mol and 1.45 for omphacite and ~84 kJ/mol and 1.12 for garnet, respectively.

COMPARISON WITH PREVIOUS WORK

Conductivity measurements at water-rich conditions in this study are based on minerals separated from the same starting eclogite as that at water-poor conditions as in the study by Liu et al. (2019). Thus, the comparison of mineral conductivity data between these reports is straightforward. For both omphacite and garnet, the conductivity systematically increases from low to high water content (**Figure 3**).

For omphacite, the samples can be classified into two groups: at water-poor conditions, the activation enthalpy is ~82 kJ/mol and the water content exponent is ~1.10 (Liu et al., 2019); at water-rich conditions, the activation enthalpy is ~70 kJ/mol and the water content exponent is ~1.45 (this study) (**Table 2**). A global fit of all the conductivity data using **Eq. 2** is unlikely. With the parameters of the low water content samples, the modeled conductivity at an assumed high water content is apparently lower than that of the measured value (**Figure 3A**). This implies different conduction mechanisms between the water-rich and water-poor conditions (see also *conduction mechanism* Section below). The conductivity of the omphacite samples, regardless of the water content, is greater than that of an Fe-free omphacite with ~50 ppm H_2O (Zhang et al., 2019). This reflects the significant role of Fe and water in enhancing omphacite conductivity (Zhang et al., 2019; Liu et al., 2021a).

For garnet, the determined activation enthalpy is similar between water-poor and water-rich conditions (**Table 2**). At water-poor conditions (40–100 ppm H_2O), the activation enthalpy is ~90 kJ/mol, and the water content exponent is ~1.07 (Liu et al., 2019); at water-rich conditions (705–1,460 ppm H_2O), the activation enthalpy is ~84 kJ/mol, and the water content exponent is ~1.12 (**Table 2**). A global fit of the conductivity data of all the samples by **Eq. 2** yields the activation enthalpy of ~87 kJ/mol and the water content exponent

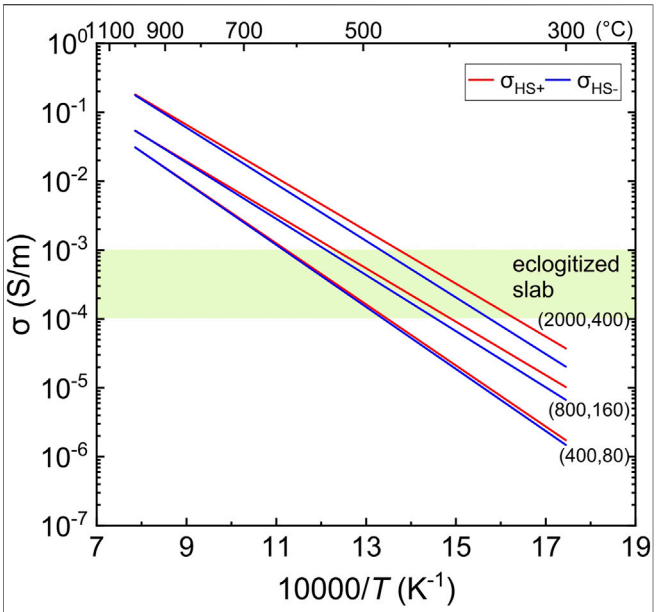

FIGURE 4 | Bulk conductivity of eclogite for a modal composition of 50% omphacite + 50% garnet. The assumed water contents are 400, 800, and 2,000 ppm H_2O for omphacite and 80, 160, and 400 ppm H_2O for garnet (see text). The shaded region marks the estimated conductivity of the eclogitized crust at 70–120 km depth by electromagnetic surveys (Vanyan et al., 2002; McGary et al., 2014; Ichiki et al., 2015; Araya Vargas et al., 2019).

of ~1.11 (**Table 2**, $r^2 > 0.97$). This may reflect the similar conduction mechanism in these garnet samples (see also *conduction mechanism* Section below). The conductivity of a pyrope garnet (Dai and Karato, 2009), with a lower Fe content (total Fe expressed as FeO of ~7.4 wt% vs. 26.5 wt% in this study) and 160 ppm H_2O, falls between our water-poor and water-rich samples, and the broadly consistent trend could be related to the more significant effect of water on conductivity.

CONDUCTION MECHANISMS

In Fe- and OH-bearing NAMs, the conduction includes the contribution from both small polarons (e.g., hopping of electron holes between Fe^{2+} and Fe^{3+}) and protons (H). The bulk conductivity is then given by $\sigma = \sigma_{Fe} + \sigma_H$, where σ_{Fe} is caused by small polaron conduction and σ_H is related to proton conduction. In most cases, $\sigma_{Fe} \ll \sigma_H$ so that $\sigma \approx \sigma_H$ (Dai and Karato, 2009; Yoshino et al., 2009; Poe et al., 2010; Yang et al., 2011, Yang et al., 2012; Yang, 2012; Yang and McCammon, 2012; Zhao and Yoshino, 2016; Liu et al., 2019; Liu et al., 2021a; Liu et al., 2021b; Zhang et al., 2019). Therefore, the main charge carriers in the omphacite and garnet samples, either water-poor (Liu et al., 2019) or water-rich (this study), are protons. The activation enthalpies of 70–90 kJ/mol (**Table 2**) are similar to those reported for proton conduction in various NAMs in the available studies noted earlier.

The different behaviors of conduction between water-poor and water-rich omphacite, concerning the activation enthalpy (~82 vs. 70 kJ/mol) and water content exponent (~1.10 vs. 1.45) as also mentioned before, suggest that the mobility of the charged protons is probably different. As documented by Jiang et al. (2022), the infrared absorption bands of structural hydroxyl in omphacite evolve with increasing temperature under otherwise identical conditions, in that the band at ~3,620 cm^{-1} is gradually enhanced and the broadening of the whole bands becomes significant. This is probably related to the temperature-driven cation rearrangements in the lattice and the transition of the space group from the ordered *P2/n* at low temperature to the disordered *C2/c* at high temperature, which influences the incorporation of water into the mineral structure (Jiang et al., 2022). The transition temperature of the space group is pressure-dependent, for example, 750°C–800°C at 1 GPa and 850°C–900°C at 2 GPa (Jiang et al., 2022). This produces different spectral shapes, and thus types, of hydroxyl between the water-rich and water-poor omphacite (**Figure 1A**) due to H-annealing at high and low temperatures (**Table 2**). The different types of water, and their possible different mobility, may lead to a difference in conductivity (**Figure 3**; **Table 2**). The incorporation mechanisms of water into omphacite have so far, however, not been resolved, as documented elsewhere (Jiang et al., 2022 and references therein). This impedes further discussion on the exact mechanism of proton movements in omphacite between water-poor and water-rich conditions.

For garnet, the conductivity at water-poor and water-rich conditions can be well-modeled by the same **Eq. 2**, indicating the similar type and mobility of the charged protons. This is supported by the similar spectral shapes of hydroxyl in the water-rich and water-poor garnet (**Figure 1B**), differing strongly from those in omphacite (**Figure 1A**). The water content exponent close to unity is similar to that reported for many NAMs, for example, clinopyroxene, orthopyroxene, plagioclase, garnet, and olivine (Yoshino et al., 2009; Yang et al., 2011; Yang et al., 2012; Yang and McCammon, 2012; Zhao and Yoshino, 2016; Liu et al., 2019; Liu et al., 2021a; Liu et al., 2021b; Zhang et al., 2019). Knowledge of the incorporation of water in garnet is key for understanding the mechanism of proton conduction. In the past, the incorporation of water in garnet was often assumed to be related to hydrogarnet defects, for example, by four protons replacing a Si^{4+} (Ackermann et al., 1983). However, recent studies show more complexity in the assignments of water in garnet, and not only Si but also Fe, Mg, and F affect water incorporation (Mosenfelder et al., 2022; Zhang et al., 2022). The difficulty in assigning the water bands makes it difficult to place further constraints on the microscale mechanism of proton conditions in garnet.

GEOPHYSICAL IMPLICATIONS

Experimental studies have shown that for a variation of several GPa only, the effect of pressure on the conductivity of omphacite and garnet in eclogite is less (Dai and Karato, 2009; Liu et al., 2021a), similar to that reported for other silicate minerals (Xu et al., 2000; Dai and Karato, 2014; Liu et al., 2021b). This ensures the modeling of the bulk conductivity of eclogite in subducting crusts. The bulk

conductivity under water-rich conditions is modeled from the constituting omphacite and garnet, following the method of Liu et al. (2019), Liu et al. (2021a). The modeling does not take into account minor accessory phases (e.g., phengite and rutile) in the matrix because they are, if present, usually texturally isolated and do not contribute to bulk conductivity. The mineral fabrics and textures, for example, aligned grains, do not influence the modeling because garnet is isotropic and the electrical anisotropy of OH-bearing clinopyroxene is negligible (Yang, 2012).

The Hashin–Shtrikman upper (σ_{HS+}) and lower (σ_{HS-}) bounds (Hashin and Shtrikman, 1963) are used to calculate the bulk conductivity:

$$\begin{aligned}\sigma_{HS+} &= \sigma_1 + \nu_2 \cdot \left[(\sigma_2 - \sigma_1)^{-1} + \nu_1/(3 \cdot \sigma_1)\right]^{-1} \\ \sigma_{HS-} &= \sigma_2 + \nu_1 \cdot \left[(\sigma_1 - \sigma_2)^{-1} + \nu_2/(3 \cdot \sigma_2)\right]^{-1}\end{aligned} \quad (3)$$

where σ_1/σ_2 and ν_1/ν_2 are the conductivity and volume fraction of the two constituents (assuming $\sigma_1>\sigma_2$), respectively. The water partition coefficient is assumed to be ~0.2 between eclogitic garnet and omphacite ($D^{Grt/Omp}$), as reported by Katayama et al. (2006). Using the parameters in **Table 2** and **Eq. 2**, the conductivities of omphacite and garnet are calculated as a function of water content by assuming 800 and 2,000 ppm H_2O in omphacite and 160 and 400 ppm H_2O in garnet. For simplification, we consider a 50% + 50% volume fraction model of omphacite and garnet, and the modeled results are given in **Figure 4**. The conductivity of water-poor eclogite, for example, 400 ppm H_2O in omphacite and 80 ppm H_2O garnet, is also calculated according to the results of Liu et al. (2019).

The modeled results demonstrate that the activation enthalpy, or slope in the Arrhenius plot (**Figure 4**), is not profoundly reduced in high water content eclogites compared to their low water content counterparts. The bulk conductivity at 600–900°C, the likely temperature of subducting crusts at 70–120 km depths, is about 0.01–0.1 S/m for water content of 2,000 ppm H_2O in omphacite and 400 ppm H_2O in garnet and is much greater at water-rich than at water-poor conditions. The general results of the modeling are unaffected by the assumed modal mineral compositions because the conductivity of omphacite and garnet at equilibrium composition is similar as documented in detail by Liu et al. (2019) and Liu et al. (2021a). The highly resistive feature of subducting crusts at 70–120 km depth, with estimated conductivities at the level of 10^{-4}–10^{-3} S/m (Vanyan et al., 2002; McGary et al., 2014; Ichiki et al., 2015; Araya Vargas et al., 2019), implies that omphacite and garnet in the eclogitized slab are unlikely to be characterized by high water content. The prevailing water content is no higher than 400 ppm H_2O and can be < 100 ppm H_2O in the two dominant minerals (**Figure 4**), if considering the composition of eclogite minerals in subducting crusts (Liu et al., 2021a). This is unaffected by the runs conducted at 1 GPa because the conductivity of hydrous omphacite and garnet increases with increasing pressure (Dai and Karato, 2009; Liu et al., 2021a) and the boundary water contents can be even lower if considering the pressure effect.

Omphacite and garnet contain > 1,500 ppm H_2O as hydroxyl groups as noted earlier. The inferred very low water content of omphacite and garnet in subducting crust suggests extremely low water activity during the eclogite–facies metamorphism and in the matrix, implying also the absence of an appreciated amount of hydrous minerals in the system (Liu et al., 2021a). This also rules out the presence of large quantities of water as isolated pockets; otherwise, the water contents of omphacite and garnet could be much higher, leading to high conductivity that is inconsistent with the geophysical surveys. Thus, our data offer support to the model of Liu et al. (2021a) that the amount of water recycled by subducting crusts to the deep mantle, for example, beyond ~70 km depth, is probably limited, although the transfer of water to shallow depths could be significant as a result of the release of pore water and breakdown of hydrous minerals in the downgoing crust (Schmidt and Poli, 2014; Cai et al., 2018).

Hydrous minerals are frequently observed in massif eclogites but could be the relics due to incomplete prograde metamorphism and/or formed by secondary events during exhumation (Fitzherbert et al., 2003; Yang et al., 2009; Brovarone et al., 2011). The documented high water contents of omphacite and garnet in massif eclogites were most likely caused by secondary fluid-related water enrichments during their transport to the Earth's surface and may not reflect those in the deep subducting crust, as pointed out also by analyses of D/H ratios and water contents (Sheng et al., 2007; Schmädicke and Gose, 2017) and conductivity measurements of water-poor eclogites (Liu et al., 2021a). The limited water recycling by subducting crusts to the deep mantle should be considered for deep water cycling. These, however, do not necessarily imply that the deep Earth is water-poor because water on the surface envelops formed by degassing of the Earth and its deep interior was already hydrous (Holland and Turekian, 2014 and references therein).

DATA AVAILABILITY STATEMENT

The original contributions presented in the study are included in the article/Supplementary Material; further inquiries can be directed to the corresponding author.

AUTHOR CONTRIBUTIONS

XY led the project. HL carried out the experiments and analyses. HL produced the plots, supervised by XY, and wrote the first draft. XY reviewed and completed the final manuscript.

FUNDING

This study was supported by the National Science Foundation of China (41725008 and 42102024), the Natural Science Foundation of Jiangsu Province (BK20210194), the Research Funds for the Frontiers Science Center for Critical Earth Material Cycling and the Fundamental Research Funds for the Central Universities.

ACKNOWLEDGMENTS

We thank the assistance of Haoran Dou for electron microprobe analyses and Kai Zhang for piston-cylinder experiments. Comments by three reviewers helped to improve the manuscript.

REFERENCES

Ackermann, L., Cemic, L., and Langer, K. (1983). Hydrogarnet Substitution in Pyrope: A Possible Location for "Water" in the Mantle. *Earth Planet. Sci. Lett.* 62, 208–214. doi:10.1016/0012-821X(83)90084-5

Araya Vargas, J., Meqbel, N. M., Ritter, O., Brasse, H., Weckmann, U., Yáñez, G., et al. (2019). Fluid Distribution in the Central Andes Subduction Zone Imaged with Magnetotellurics. *J. Geophys. Res. Solid Earth* 124, 4017–4034. doi:10.1029/2018JB016933

Brovarone, A. V., Groppo, C., Hetényi, G., Compagnoni, R., and Malavieille, J. (2011). Coexistence of Lawsonite-Bearing Eclogite and Blueschist: Phase Equilibria Modelling of Alpine Corsica Metabasalts and Petrological Evolution of Subducting Slabs. *J. Metamorph. Geol.* 29, 583–600. doi:10.1111/j.1525-1314.2011.00931.x

Cai, C., Wiens, D. A., Shen, W., and Eimer, M. (2018). Water Input into the Mariana Subduction Zone Estimated from Ocean-Bottom Seismic Data. *Nature* 563, 389–392. doi:10.1038/s41586-018-0655-4

Dai, L., and Karato, S.-i. (2009). Electrical Conductivity of Pyrope-Rich Garnet at High Temperature and High Pressure. *Phys. Earth Planet. Inter.* 176, 83–88. doi:10.1016/j.pepi.2009.04.002

Dai, L., and Karato, S.-i. (2014). The Effect of Pressure on the Electrical Conductivity of Olivine under the Hydrogen-Rich Conditions. *Phys. Earth Planet. Inter.* 232, 51–56. doi:10.1016/j.pepi.2014.03.010

Fitzherbert, J. A., Clarke, G. L., and Powell, R. (2003). Lawsonite-Omphacite-Bearing Metabasites of the Pam Peninsula: NE New Caledonia: Evidence for Disrupted Blueschist- to Eclogite-Facies Conditions. *J. Petrol.* 44, 1805–1831. doi:10.1093/petrology/egg060

Franz, G., Thomas, S., and Smith, D. C. (1986). High-pressure Phengite Decomposition in the Weissenstein Eclogite, Münchberger Gneiss Massif, Germany. *Contrib. Mineral. Pet.* 92, 71–85. doi:10.1007/BF00373964

Hashin, Z., and Shtrikman, S. (1963). A Variational Approach to the Theory of the Elastic Behaviour of Multiphase Materials. *J. Mech. Phys. Solids* 11, 127–140. doi:10.1016/0022-5096(63)90060-7

Holland, H. D., and Turekian, K. K. (2014). *Treatise on Geochemistry: Volume 1 Meteorites and Cosmochemical Processes*. 2nd ed.. Oxford: Elsevier.

Huebner, J. S., and Dillenburg, R. G. (1995). Impedance Spectra of Hot, Dry Silicate Minerals and Rock; Qualitative Interpretation of Spectra. *Am. Mineral.* 80, 46–64. doi:10.2138/am-1995-1-206

Ichiki, M., Ogawa, Y., Kaida, T., Koyama, T., Uyeshima, M., Demachi, T., et al. (2015). Electrical Image of Subduction Zone beneath Northeastern Japan. *J. Geophys. Res. Solid Earth* 120, 7937–7965. doi:10.1002/2015JB012028

Jiang, P., Liu, H., Skogby, H., Chen, R.-X., and Yang, X. (2022). Water in Omphacite Fingerprints the Thermal History of Eclogites. *Geology* 50, 316–320. doi:10.1130/g49566.1

Karato, S.-i. (2006). "Remote Sensing of Hydrogen in Earth's Mantle," in *Water Nominally Anhydrous Minerals*. Editors H. Keppler and J. R. Smyth (Mineralogical Society of America), 343–376. doi:10.1515/9781501509476-019

Katayama, I., and Nakashima, S. (2003). Hydroxyl in Clinopyroxene from the Deep Subducted Crust: Evidence for H_2O Transport into the Mantle. *Am. Mineral.* 88, 229–234. doi:10.2138/am-2003-0126

Katayama, I., Nakashima, S., and Yurimoto, H. (2006). Water Content in Natural Eclogite and Implication for Water Transport into the Deep Upper Mantle. *Lithos* 86, 245–259. doi:10.1016/j.lithos.2005.06.006

Langer, K., Robarick, E., Sobolev, N. V., Shatsky, V. S., and Wang, W. (1993). Single-Crystal Spectra of Garnets from Diamondiferous High-Pressure Metamorphic Rocks from Kazakhstan: Indications for OH-, H_2O, and FeTi Charge Transfer. *Eur. J. Mineral.* 5, 1091–1100. doi:10.1127/ejm/5/6/1091

Li, Y., Yang, X., Yu, J.-H., and Cai, Y.-F. (2016). Unusually High Electrical Conductivity of Phlogopite: the Possible Role of Fluorine and Geophysical Implications. *Contrib. Mineral. Pet.* 171, 37. doi:10.1007/s00410-016-1252-x

Li, Y., Jiang, H., and Yang, X. (2017). Fluorine Follows Water: Effect on Electrical Conductivity of Silicate Minerals by Experimental Constraints from Phlogopite. *Geochim. Cosmochim. Acta* 217, 16–27. doi:10.1016/j.gca.2017.08.020

Liu, H., Zhu, Q., and Yang, X. (2019). Electrical Conductivity of OH-bearing Omphacite and Garnet in Eclogite: the Quantitative Dependence on Water Content. *Contrib. Mineral. Pet.* 174, 57. doi:10.1007/s00410-019-1593-3

Liu, H., Zhang, K., Ingrin, J., and Yang, X. (2021a). Electrical Conductivity of Omphacite and Garnet Indicates Limited Deep Water Recycling by Crust Subduction. *Earth Planet. Sci. Lett.* 559, 116784. doi:10.1016/j.epsl.2021.116784

Liu, H., Zhu, Q., Xu, X., Fei, H., and Yang, X. (2021b). High Electrical Conductivity of Olivine at Oxidizing Conditions of the Shallow Mantle and Geophysical Implications. *JGR Solid Earth* 126, e2021JB022739. doi:10.1029/2021JB022739

McGary, R. S., Evans, R. L., Wannamaker, P. E., Elsenbeck, J., and Rondenay, S. (2014). Pathway from Subducting Slab to Surface for Melt and Fluids beneath Mount Rainier. *Nature* 511, 338–340. doi:10.1038/nature13493

Mosenfelder, J. L., von der Handt, A., Withers, A. C., Bureau, H., Raepsaet, C., and Rossman, G. R. (2022). Coupled Hydrogen and Fluorine Incorporation in Garnet: New Constraints from FTIR, ERDA, SIMS, and EPMA. *Am. Mineral.* 107, 587–602. doi:10.2138/am-2021-7880

Poe, B. T., Romano, C., Nestola, F., and Smyth, J. R. (2010). Electrical Conductivity Anisotropy of Dry and Hydrous Olivine at 8 GPa. *Phys. Earth Planet. Inter.* 181, 103–111. doi:10.1016/j.pepi.2010.05.003

Qiu, Y., Jiang, H., Kovács, I., Xia, Q. K., and Yang, X. (2018). Quantitative Analysis of H-Species in Anisotropic Minerals by Unpolarized Infrared Spectroscopy: An Experimental Evaluation. *Am. Mineral.* 103, 1761–1769. doi:10.2138/am-2018-6620

Schmädicke, E., and Gose, J. (2017). Water Transport by Subduction: Clues from Garnet of Erzgebirge UHP Eclogite. *Am. Mineral.* 102, 975–986. doi:10.2138/am-2017-5920

Schmidt, M. W., and Poli, S. (2014). "Devolatilization during Subduction," in *Treatise on Geochemistry*. Second Edition, 669–701. doi:10.1016/B978-0-08-095975-7.00321-1

Sheng, Y.-M., Xia, Q.-K., Dallai, L., Yang, X.-Z., and Hao, Y.-T. (2007). H_2O Contents and D/H Ratios of Nominally Anhydrous Minerals from Ultrahigh-Pressure Eclogites of the Dabie Orogen, Eastern China. *Geochim. Cosmochim. Acta* 71, 2079–2103. doi:10.1016/j.gca.2007.01.018

Shuai, K., and Yang, X. (2017). Quantitative Analysis of H-Species in Anisotropic Minerals by Polarized Infrared Spectroscopy along Three Orthogonal Directions. *Contrib. Mineral. Pet.* 172, 14. doi:10.1007/s00410-017-1336-2

Vanyan, L. L., Berdichevsky, M. N., Pushkarev, P. Y., and Romanyuk, T. V. (2002). A Geoelectric Model of the Cascadia Subduction Zone. *Izv. Phys. Solid Earth* 38, 816–845.

Xia, Q.-K., Sheng, Y.-M., Yang, X.-Z., and Yu, H.-M. (2005). Heterogeneity of Water in Garnets from UHP Eclogites, Eastern Dabieshan, China. *Chem. Geol.* 224, 237–246. doi:10.1016/j.chemgeo.2005.08.003

Xu, Y., Shankland, T. J., and Duba, A. G. (2000). Pressure Effect on Electrical Conductivity of Mantle Olivine. *Phys. Earth Planet. Inter.* 118, 149–161. doi:10.1016/S0031-9201(99)00135-1

Yang, J., Xu, Z., Li, Z., Xu, X., Li, T., Ren, Y., et al. (2009). Discovery of an Eclogite Belt in the Lhasa Block, Tibet: A New Border for Paleo-Tethys? *J. Asian Earth Sci.* 34, 76–89. doi:10.1016/j.jseaes.2008.04.001

Yang, X., and McCammon, C. (2012). Fe^{3+}-rich Augite and High Electrical Conductivity in the Deep Lithosphere. *Geology* 40, 131–134. doi:10.1130/G32725.1

Yang, X., Keppler, H., McCammon, C., Ni, H., Xia, Q., and Fan, Q. (2011). Effect of Water on the Electrical Conductivity of Lower Crustal Clinopyroxene. *J. Geophys. Res.* 116, B04208. doi:10.1029/2010JB008010

Yang, X., Keppler, H., McCammon, C., and Ni, H. (2012). Electrical Conductivity of Orthopyroxene and Plagioclase in the Lower Crust. *Contrib. Mineral. Pet.* 163, 33–48. doi:10.1007/s00410-011-0657-9

Yang, X. (2012). Orientation-related Electrical Conductivity of Hydrous Olivine, Clinopyroxene and Plagioclase and Implications for the Structure of the Lower Continental Crust and Uppermost Mantle. *Earth Planet. Sci. Lett.* 317-318, 241–250. doi:10.1016/j.epsl.2011.11.011

Yoshino, T., Manthilake, G., Matsuzaki, T., and Katsura, T. (2008). Dry Mantle Transition Zone Inferred from the Conductivity of Wadsleyite and Ringwoodite. *Nature* 451, 326–329. doi:10.1038/nature06427

Yoshino, T., Matsuzaki, T., Shatskiy, A., and Katsura, T. (2009). The Effect of Water on the Electrical Conductivity of Olivine Aggregates and its Implications for the Electrical Structure of the Upper Mantle. *Earth Planet. Sci. Lett.* 288, 291–300. doi:10.1016/j.epsl.2009.09.032

Zhang, B., Zhao, C., Ge, J., and Yoshino, T. (2019). Electrical Conductivity of Omphacite as a Function of Water Content and Implications for High

Conductivity Anomalies in the Dabie-Sulu UHPM Belts and Tibet. *J. Geophys. Res. Solid Earth* 124, 12523–12536. doi:10.1029/2019JB018826

Zhang, K., Liu, H., Ionov, D. A., and Yang, X. (2022). Effects of Oxygen Fugacity on Hydroxyl Incorporation in Garnet at 1-3 GPa and 800-1000°C and Implications for Water Storage in the Mantle. *JGR Solid Earth* 127, e2022JB023948. doi:10.1029/2022jb023948

Zhao, C., and Yoshino, T. (2016). Electrical Conductivity of Mantle Clinopyroxene as a Function of Water Content and its Implication on Electrical Structure of Uppermost Mantle. *Earth Planet. Sci. Lett.* 447, 1–9. doi:10.1016/j.epsl.2016.04.028

Conflict of Interest: The authors declare that the research was conducted in the absence of any commercial or financial relationships that could be construed as a potential conflict of interest.

Publisher's Note: All claims expressed in this article are solely those of the authors and do not necessarily represent those of their affiliated organizations, or those of the publisher, the editors, and the reviewers. Any product that may be evaluated in this article, or claim that may be made by its manufacturer, is not guaranteed or endorsed by the publisher.